RESEARCH ARTICLE | APRIL 21 2026

Viscous gravity currents with linear basal slip in planar and axisymmetric geometries

Bruno Rossi ; Vittorio Di Federico

Physics of Fluids 38, 043111 (2026)
https://doi.org/10.1063/5.0320767

Physics of Fluids ARTICLE pubs.aip.org/aip/pof

Viscous gravity currents with linear basal slip in planar and axisymmetric geometries

Cite as: Phys. Fluids **38**, 043111 (2026); doi: 10.1063/5.0320767
Submitted: 2 January 2026 · Accepted: 6 April 2026 ·
Published Online: 21 April 2026

Bruno Rossi[a] and Vittorio Di Federico

AFFILIATIONS

Department of Civil, Chemical, Environmental, and Materials Engineering, Alma Mater Studiorum—Università di Bologna, Viale Risorgimento 2, 40136 Bologna, Italy

[a]Author to whom correspondence should be addressed: bruno.rossi2@unibo.it

ABSTRACT

We investigate the impact of basal sliding on the spreading of a viscous Newtonian gravity current (GC) propagating over a slippery substrate, under the lubrication approximation and assuming laminar flow. The current volume is assumed to vary in time according to a power-law injection protocol. The basal slip is modeled through a Navier slip condition, introducing a nonzero slip velocity at the base of the current. This results in an additional contribution to the governing partial differential equation, which in the dimensionless form depends on a slip number N_s. This parameter encapsulates the injection protocol, fluid properties, and slip length and quantifies the relative importance of basal sliding. A unified theoretical formulation valid for both planar and axisymmetric geometries is derived. Within this framework, similarity solutions exist only in two asymptotic regimes: a no-slip limit, which recovers classical results from the literature, and a very-slippery limit, for which new similarity solutions are obtained. The transient regime connecting these limits is resolved using a fully numerical integration scheme. Comparisons between numerical and asymptotic solutions show that their range of validity depends on time, geometry, and the values of the injection exponent and slip number. A dimensional case study describing the spreading of a fluid with a macroscopic slip length illustrates that the presence of a highly slippery substrate strongly influences the current propagation, while for microscopic slip lengths, basal sliding becomes dynamically relevant primarily for micro-scale GCs. Finally, the role of alternative nondimensionalizations and typical ranges of slip numbers inferred from experimental data are discussed in dedicated appendices.

I. INTRODUCTION

Understanding the motion of a fluid that intrudes into another is essential for modeling a wide range of natural and anthropogenic processes. When the flow is driven by a density difference between the intruding and the ambient saturating fluid, i.e., by buoyancy forces, a gravity current (GC) arises. This framework can be adapted to study the origin of atmospheric phenomena, such as squalls during thunderstorms, or to model the evolution of airborne snow avalanches in mountainous regions.[1] Environmental pollution problems, such as oil spills on the sea surface, are also examples of anthropogenic gravity currents propagating over a denser fluid. This wide range of applications, together with the multiplicity and intrinsic variability of boundary conditions in natural contexts, continues to stimulate extensive research on gravity currents. Recent studies have applied gravity current theory to investigate the effects of vegetation-induced drag forces on water propagation in channels with different geometries,[2] as well as to assess the impact of surface irregularities that commonly characterize the substrates over which gravity currents propagate in natural environments.[3]

Classical gravity current theory, however, relies on a number of simplifying assumptions. Gravity currents are typically classified as viscous when their propagation is governed by a balance between viscous and buoyancy forces, with inertial effects being negligible, or as inertial when a buoyancy–inertia balance dominates. Lava flows, mudflows, and currents generated by effluent discharges into rivers or lakes often evolve in the viscous regime.[4] Furthermore, the flow is commonly assumed to satisfy the lubrication approximation, whereby the current is modeled as a thin film whose thickness is much smaller than its horizontal extent. Under this assumption, vertical accelerations are neglected and the pressure field is hydrostatic, while the ambient fluid is treated as quiescent.[5] Capillary effects and mixing between the two fluids are also conventionally neglected. Such assumptions render the gravity current problem amenable to similarity solutions, which are valid as intermediate asymptotics in a wide

range of configurations. Examples include viscous gravity currents spreading in converging fractures or channels with varying cross sections,[6–8] currents propagating upslope,[9] and gravity currents advancing through vegetation-like obstacles.[10] In these studies, the existence of self-similar solutions relies critically on idealized boundary conditions and simplified flow physics, which facilitate analytical progress but may not always capture the complexity of natural systems.

Another key assumption commonly adopted in gravity current modeling is the no-slip boundary condition, namely, the velocity of the current is assumed to vanish at the liquid–solid interphase. This assumption is often appropriate in laboratory experiments, where gravity currents propagate over rigid substrates.[11] However, many natural fluid–mechanical systems do not obey the no-slip condition and instead exhibit basal sliding. This behavior has been observed, for example, in many glaciers, for which sliding laws have been proposed to describe motion induced by the presence of a thin subglacial till.[12,13] Such wall slippage is usually characterized by introducing a slip length $\bar{k}$, which is defined as the distance below the wall at which the linear extrapolation of the near-wall velocity profile vanishes.[14]

However, such basal sliding is challenging to reproduce under laboratory conditions. Among the various approaches developed to relax the no-slip condition in laboratory experiments, Yan and Kowal[11] proposed a method to generate effective slip by studying the propagation of a viscous gravity current over a slippery substrate composed of an array of square cavities saturated with a less viscous fluid. As the current advances, the shear stress exerted on the underlying fluid induces a recirculating flow within each cavity, giving rise to a finite slip velocity at the interface between the two fluids. This configuration enabled the emergence of a macroscopic linear sliding law, which is homogeneous at the large scale. On this basis, the authors derived similarity solutions for the spreading of a fluid injected at a constant rate in planar geometry, identifying two asymptotic regimes: a highly slippery regime and a no-slip regime, which were shown to govern the dynamics at early and late times, respectively.

In this work, we extend and generalize the theoretical results of Yan and Kowal[11] by investigating the impact of basal sliding on a gravity current propagating over a flat and rigid surface in both planar and axisymmetric geometries. The novelty of the present study lies in the adoption of a unified formulation valid for both geometries, together with the introduction of a generic power-law injection condition characterized by a non-negative exponent α, in place of a constant injection rate. Within this framework, a dam-break release corresponds to $\alpha = 0$, while constant-flux injection is recovered as the special case $\alpha = 1$.

The presence of basal slip is modeled through a linear relation between slip velocity and shear stress, which is equivalent to adopting a Navier slip law. Under this condition, the resulting governing equation does not generally admit similarity solutions. Accordingly, self-similar solutions are obtained only in the limiting cases of very-slippery and no-slip conditions, while the intermediate transient regime is resolved through direct numerical integration of the governing equation.

We show that the temporal window over which the very-slippery solution accurately describes the gravity current dynamics depends sensitively on the problem parameters, and that, for the time scales relevant to fluid injection and laboratory observations, pronounced effects of basal sliding arise primarily for micro-scale gravity currents or for highly slippery substrates, as the one reproduced by Yan and Kowal.[11] Large-scale slip-dominated phenomena, such as glacier motion, are, therefore, beyond the scope of the present study, as they would manifest over much longer time scales and involve additional physical processes, including thermodynamic effects.

The remainder of the paper is organized as follows: In Sec. II, we present the theoretical formulation of the problem in both dimensional and dimensionless forms. Section III develops self-similar solutions for the very-slippery and no-slip regimes. In Sec. IV, the transient regime is addressed through a fully numerical approach, and the resulting current profiles are compared with the semi-analytical solutions. Section V presents a numerical example illustrating the impact of basal sliding on the propagation of a real fluid. Finally, Sec. VI summarizes the main findings and provides concluding remarks.

II. FORMULATION OF THE PROBLEM

We consider a gravity current propagating over a slippery substrate under the lubrication approximation. Basal sliding induces a finite slip velocity u_s at the base of the current, as depicted in Fig. 1. In order to treat both planar and axisymmetric configurations within a unified framework, the coordinate x is used to denote the horizontal direction in both geometries.

Under the thin-current hypothesis, vertical velocity components are negligible compared to horizontal ones, and the pressure distribution within the current is, therefore, hydrostatic, as originally discussed by Huppert.[15] The flow is governed by a balance between buoyancy and viscous forces, while inertial effects are neglected, leading to the simplified one-dimensional momentum equation

$$\frac{1}{\rho}\frac{\partial p}{\partial x} = \nu \frac{\partial^2 u}{\partial z^2}, \tag{1}$$

where ρ ($[ML^{-3}]$) and ν ($[L^2T^{-1}]$) are the density and kinematic viscosity of the fluid, respectively, and $u = u(x, z, t)$ is the horizontal velocity of the current.

To determine the velocity profile of the current, we introduce the boundary conditions

$$u(x, 0, t) = u_s; \quad \left.\frac{\partial u}{\partial z}\right|_h = 0, \tag{2}$$

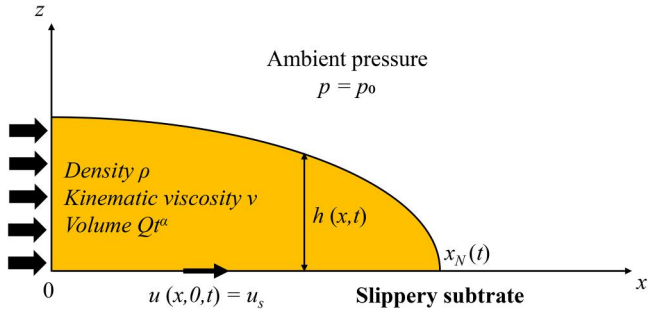

FIG. 1. Sketch of a gravity current spreading over a slippery substrate. Basal sliding is represented by a slip velocity u_s at the base of the gravity current.

where the classical no-slip assumption $u(z=0)=0$ is replaced by a finite slip velocity u_s at the base of the gravity current. The second condition enforces continuity of the shear stress at the top of the current.[15] Integration of Eq. (1) with the boundary conditions (2) yields

$$u = -\frac{1}{2}\frac{g}{\nu} z(2h-z)\frac{\partial h}{\partial x} + u_s. \tag{3}$$

We model basal sliding through a Navier slip condition

$$u_s = \bar{k}\left.\frac{\partial u}{\partial z}\right|_{z=0}, \tag{4}$$

where $\bar{k}$ is the slip length, which can be determined experimentally (see Appendix A for a detailed overview of typical values of $\bar{k}$). Substituting the velocity profile (3) into the local mass balance equation,

$$\frac{\partial h}{\partial t} = -\frac{1}{x^d}\frac{\partial}{\partial x}\left(x^d \int_0^h u\,dz\right), \tag{5}$$

where $d=0$ and $d=1$ correspond to planar and axisymmetric geometries, respectively, and introducing the slip condition (4) yields

$$\frac{\partial h}{\partial t} = \frac{g}{\nu}\frac{1}{x^d}\frac{\partial}{\partial x}\left(\frac{1}{3}x^d h^3\frac{\partial h}{\partial x} + \bar{k}x^d h^2\frac{\partial h}{\partial x}\right), \tag{6}$$

which follows from the expression of the shear stress at the slippery bottom and from the hydrostatic pressure distribution [see Eq. (2.15) of Yan and Kowal[11]]. Equation (6) constitutes the governing partial differential equation (PDE) for a viscous gravity current with basal slip, valid for both planar ($d=0$) and axisymmetric ($d=1$) geometries. In the right-hand side of the equation, the first term within parentheses corresponds to the classical no-slip contribution and reduces to Eqs. (2.9) and (2.21) of Huppert[15] for planar and axisymmetric geometries, respectively; the second term is an additional contribution arising from the inclusion of basal sliding. Note that Eq. (6) is derived under the assumption of negligible capillary forces. This hypothesis is valid whenever the Bond number $B=\rho g L^2/\sigma \gg 1$, as discussed by Huppert,[16] where L is a characteristic length scale of the current and σ is the surface tension. The validity of this condition will be assessed in further analyses. The other underlying assumption is that shear stresses dominate over extensional stresses, which is valid under the thin-film approximation $h/l \ll 1$ (h/l is the aspect ratio of the current with l being its horizontal extension), as $\partial u/\partial z \sim u/h$ and $\partial u/\partial x \sim u/l$.

To complete the formulation of the problem, we impose global mass conservation together with a boundary condition at the current front ($x=x_N$),

$$(2\pi)^d \int_0^{x_N} x^d h\,dx = Qt^\alpha; \quad h(x_N,t)=0, \tag{7}$$

where Q has dimensions $[L^{d+2}T^{-\alpha}]$ and the exponent α characterizes the type of injection. In particular, $\alpha=0$ represents the release of a finite volume (dam-break) and $\alpha=1$ stands for constant-flux injection while $\alpha=2$ is representative of a linearly increasing flow rate.

To solve this differential problem, we recast it in dimensionless form by introducing the variables

$$H=\frac{h}{x_0}; \quad X=\frac{x}{x_0}; \quad X_N=\frac{x_N}{x_0}; \quad T=\frac{t}{t_0}, \tag{8}$$

where the characteristic length and time scales are defined as

$$x_0 = \left(\left(\frac{\nu}{g}\right)^\alpha Q\right)^{\frac{1}{\alpha+(d+2)}}; \quad t_0 = \left(\left(\frac{\nu}{g}\right)^{d+2}\frac{1}{Q}\right)^{\frac{1}{\alpha+(d+2)}}. \tag{9}$$

These scales are chosen following Lister,[17] and the associated velocity scale is $u_0=x_0/t_0$. Our choice of length scales is in variance with Yan and Kowal,[11] who used the slip length as the vertical scale. The implications of employing different nondimensionalizations are discussed in Appendix B. Substituting the characteristic scales defined in Eq. (9) into Eqs. (6) and (7) yields the following non-dimensional form of the governing problem

$$\frac{\partial H}{\partial T} = \frac{1}{X^d}\frac{\partial}{\partial X}\left(\frac{1}{3}X^d H^3\frac{\partial H}{\partial X} + N_s X^d H^2\frac{\partial H}{\partial X}\right), \tag{10}$$

together with the global mass constraint and front condition

$$(2\pi)^d \int_0^{X_N} X^d H\,dX = T^\alpha; \quad H(X_N,T)=0. \tag{11}$$

Here,

$$N_s = \frac{\bar{k}}{x_0} = \bar{k}\left[\left(\frac{\nu}{g}\right)^\alpha Q\right]^{-\frac{1}{\alpha+(d+2)}} \tag{12}$$

is a dimensionless slip number that measures the relative magnitude of the slip length with respect to the characteristic horizontal length scale.

The dimensionless problem (10) and (11) is not generally amenable to a similarity solution, due to the additional term arising from basal slip. Therefore, in Sec. III, we look for similarity transformations to solve the problem in two asymptotic regimes. In the no-slip limit, where the first term in Eq. (10) dominates, the solutions reduce to the classical results of Huppert.[15] In the opposite, very-slippery limit, where the slip-induced contribution prevails, we derive similarity solutions that extend the analysis of Yan and Kowal,[11] previously restricted to two-dimensional spreading under constant-flux injection ($d=0$ and $\alpha=1$). The intermediate transient regime connecting these two limits is addressed in Sec. IV through direct numerical integration of the governing partial differential equation using an explicit time-marching scheme.

III. SIMILARITY SOLUTIONS

In this section, we solve the differential problem (10) and (11) in two limiting cases: the absence of basal sliding (A) and the regime in which slip dominates the gravity current dynamics (B). In both cases, the governing partial differential equation is reduced to an ordinary differential equation (ODE) by introducing appropriate similarity scalings.

A. No-slip limit ($H \gg N_s$)

We first investigate the regime corresponding to the no-slip assumption. This asymptotic limit applies when the first term of Eq. (10) dominates the slip-induced contribution, namely, when

$H^3 \gg N_s H^2$, or equivalently $H \gg N_s$, in dimensionless terms. The validity of this condition depends on the injection protocol, as characterized by the exponent α, and may occur at early or late times during the evolution of the current. For example, in the case of a finite-volume release ($\alpha = 0$), this regime is expected to be representative at early times, when the current is still relatively thick and has not yet significantly flattened during its propagation. More generally, however, the applicability of the no-slip regime depends not only on the injection protocol but also on the value of the slip number N_s: larger values of N_s enhance the relative importance of basal sliding. The temporal ranges over which this assumption holds are discussed later and differ from those reported by Yan and Kowal,[11] owing to the different nondimensionalization adopted here, as detailed in Appendix B. Nevertheless, when expressed in the dimensional form, both nondimensionalization approaches yield the same condition for the validity of the no-slip limit, namely, $h \gg \overline{k}$. To determine similarity solutions to (10) and (11) in the no-slip limit, we introduce the similarity scalings

$$\xi = XT^{-\frac{3\alpha+1}{5+3d}}; \quad H = \xi_N^{2/3} T^{\frac{(2-d)\alpha-1}{5-d}} \Phi(\zeta), \tag{13}$$

where $\zeta = \xi/\xi_N$ is the rescaled similarity variable and Φ is the shape function, which is representative of the dimensionless height of the current. Upon introducing the similarity variables in Eqs. (10) and (11) the problem reduces to the following ordinary differential equation for the shape function $\Phi(\zeta)$:

$$\frac{d}{d\zeta}\left[\frac{1}{3}\zeta^d \Phi^3 \frac{d\Phi}{d\zeta}\right] + \left(\frac{3\alpha+1}{5+3d}\right)\zeta^{d+1}\frac{d\Phi}{d\zeta} - \left(\frac{(2-d)\alpha-1}{5-d}\right)\zeta^d \Phi = 0, \tag{14}$$

together with the normalization condition fixing the current extent and the boundary condition at the front

$$\xi_N = \left[(2\pi)^d \int_0^1 \zeta^d \Phi(\zeta) d\zeta\right]^{-\frac{3}{5+3d}}; \quad \Phi(1) = 0. \tag{15}$$

For $\alpha = 0$, the problem admits the following closed form solution

$$\Phi(\zeta) = \left(\frac{9}{2(5+3d)}\right)^{1/3} (1-\zeta^2)^{1/3}. \tag{16}$$

As expected, for $d = 0$ or $d = 1$, Eq. (14) coincides with Eqs. (2.13) or (2.25) of Huppert,[15] respectively, except for the prefactor $1/3$ in the first term between parentheses, which arises from the nondimensionalization process.

For $\alpha \neq 0$, the differential problem (14) and (15) does not admit an analytical solution and can only be solved numerically. In addition to the boundary condition $\Phi(1) = 0$, a second condition is required to integrate the ordinary differential equation. This condition is obtained by approximating the behavior of the shape function near the current front using a Frobenius expansion. Retaining the leading-order terms yields

$$\Phi(\zeta) = \left(9\left(\frac{3\alpha+1}{5+3d}\right)\right)^{1/3} (1-\zeta)^{1/3}\left[1 + \frac{3\alpha-(4-3d)}{6(4-3d)(3\alpha+1)}(1-\zeta)\right], \tag{17}$$

which captures the asymptotic behavior of the solution as $\zeta \to 1$. Defining

$$A = \left[9\left(\frac{3\alpha+1}{5+3d}\right)\right]^{1/3}, \tag{18}$$

the corresponding expression for the derivative of the shape function at the current front is

$$\left.\frac{d\Phi}{d\zeta}\right|_{\zeta\to 1} = -\frac{A}{3}(1-\zeta)^{-2/3}. \tag{19}$$

B. Very-slippery limit ($H \ll N_s$)

We now consider the opposite asymptotic regime, which arises when the slip contribution in Eq. (10) dominates the no-slip term, i.e., $H^3 \ll N_s H^2$ or equivalently $H \ll N_s$ in dimensionless terms or alternatively $h \ll \overline{k}$ in dimensional variables. Again, the temporal validity of this regime depends on both the injection exponent α and the slip number N_s and may, therefore, occur at early or late stages of the flow evolution: for a finite-volume release ($\alpha = 0$), the very-slippery limit is expected to become relevant at long times, as the gravity current progressively thins during its propagation. In contrast, for $\alpha \geq 1$, slip effects are anticipated to dominate the early stages of gravity current evolution.

We derive similarity solutions in the very-slippery limit by defining the following self-similar scalings

$$\xi = XT^{-\frac{2\alpha+1}{4+2d}}; \quad H = N_s^{-1/2} \xi_N T^{\frac{(2-d)\alpha-1}{4-d}} \Phi(\zeta), \tag{20}$$

where, as before, $\zeta = \xi/\xi_N$. Substitution of these scalings into Eqs. (10) and (11) reduces the governing problem to

$$\frac{d}{d\zeta}\left[\zeta^d \Phi^2 \frac{d\Phi}{d\zeta}\right] + \left(\frac{2\alpha+1}{4+2d}\right)\zeta^{d+1}\frac{d\Phi}{d\zeta} - \left(\frac{(2-d)\alpha-1}{4-d}\right)\zeta^d \Phi = 0, \tag{21}$$

$$\xi_N = \left[\frac{(2\pi)^d}{\sqrt{N_s}} \int_0^1 \zeta^d \Phi(\zeta) d\zeta\right]^{\frac{1}{2+d}}; \quad \Phi(1) = 0. \tag{22}$$

For the special case $\alpha = 0$, the problem admits the analytical solution

$$\Phi(\zeta) = \frac{1}{\sqrt{4+2d}}\sqrt{1-\zeta^2}. \tag{23}$$

As for the no-slip case, solving the ordinary differential equation (21) requires an additional boundary condition. The latter is obtained by performing a Frobenius expansion of the shape function $\Phi(\zeta)$ near the current front. Retaining the leading-order terms yields the following approximation

$$\Phi(\zeta) = \left(\frac{2\alpha+1}{2+d}\right)^{1/2} (1-\zeta)^{1/2}\left[1 + \frac{2(\alpha+d)-3}{2(6-4d)(2\alpha+1)}(1-\zeta)\right], \tag{24}$$

which describes the local behavior of the solution as $\zeta \to 1$. Defining

$$B = \left(\frac{2\alpha+1}{2+d}\right)^{1/2}, \tag{25}$$

the corresponding asymptotic expression for the derivative at the front is

$$\left.\frac{d\Phi}{d\zeta}\right|_{\zeta\to 1} = -\frac{B}{2}(1-\zeta)^{-1/2}. \tag{26}$$

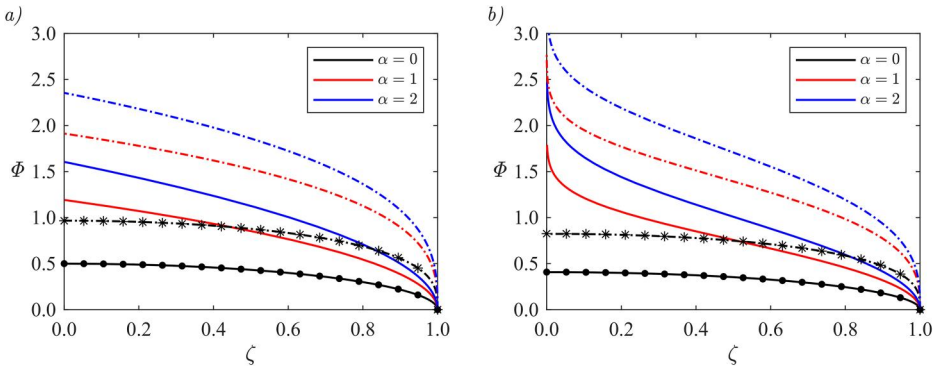

FIG. 2. Shape function Φ vs the scaled similarity variable ζ for (a) planar geometry and (b) axisymmetric geometry. Dashed and continuous lines correspond to no-slip and very-slippery regimes, respectively, and they are obtained through numerical integration of Eqs. (14) and (21). Black stars and dots are the graphical representation of the analytical solutions (16)–(23).

The integration of the ODEs (14) and (21) allows the representation of the shape function Φ for different values of the injection exponent α, as shown in Fig. 2. Analytical solutions (16)–(23) derived for $\alpha = 0$ are also reported, showing a perfect overlap with the numerical integration. Note that the scaling introduced in Eq. (20) makes the very-slippery shape function independent from the slip number N_s. Figure 3 shows the average thickness $\overline{H}$ of the GC under the no-slip and very-slippery assumptions for different values of α and N_s. In plane geometry, the no-slip assumption is valid at early times for $\alpha = 0$ whereas it becomes the dominant regime at late times for $\alpha = 1$ and 2. Moreover, as N_s increases, the very-slippery solution travels farther distances for the same value of T, resulting in a smaller value of $\overline{H}$, as predicted by the second expression of Eq. (20). The same behavior holds in radial geometry, where $\overline{H}$ values are lower than the corresponding planar ones at the same T as the GC spreads over a larger surface. However, note that for $\alpha = 1$ the average current height remains constant over time in both asymptotic regimes, in agreement with Eqs. (13) and (20). Looking at Fig. 3(c), this means that the very-slippery solution is never able to reproduce the real propagation of the GC, as $\overline{H} \approx 2 \gg N_s = 0.01$. The opposite happens in Fig. 3(d), where the no-slip solution predicts an average thickness of $\overline{H} \approx 0.8 < 1$; thus, the current will evolve in the very-slippery asymptotic. In general, this is so since similarity solutions describe only the limiting regimes in which either the no-slip or slip contribution dominates. To capture the full evolution of the gravity current when both mechanisms are simultaneously relevant, it is necessary to resort to numerical methods and directly integrate the governing differential problem to resolve the transient regime.

The similarity transformations (13) and (20) predict the front position to evolve as

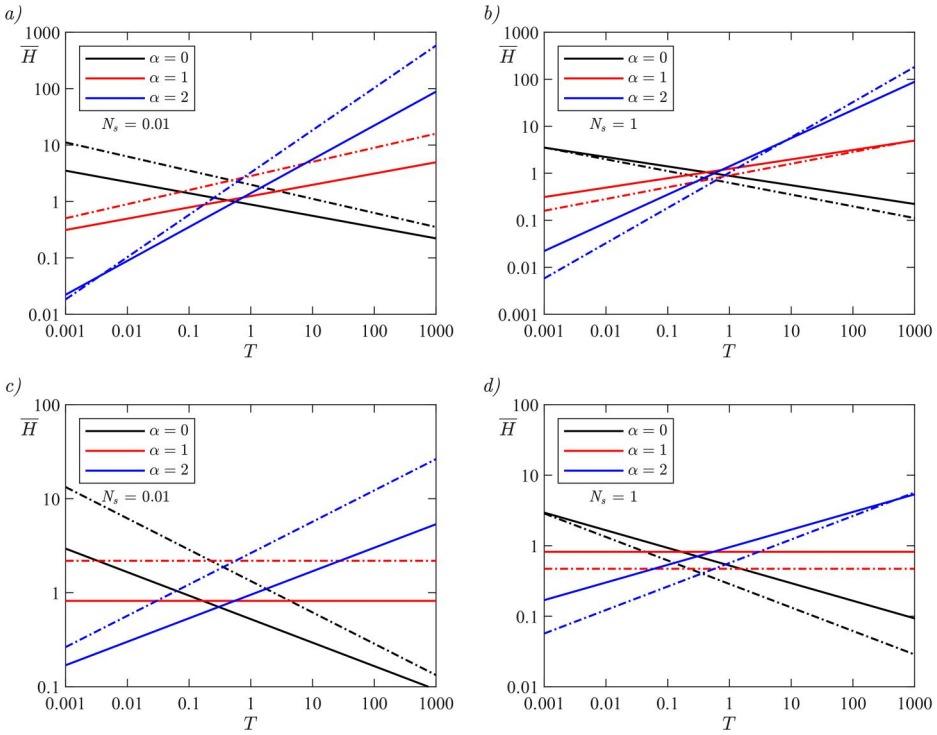

FIG. 3. Dimensionless current average thickness $\overline{H}$ vs dimensionless time T under no-slip (continuous lines) and very-slippery (dashed lines) regimes. Top and bottom rows refer to plane and radial coordinates, respectively.

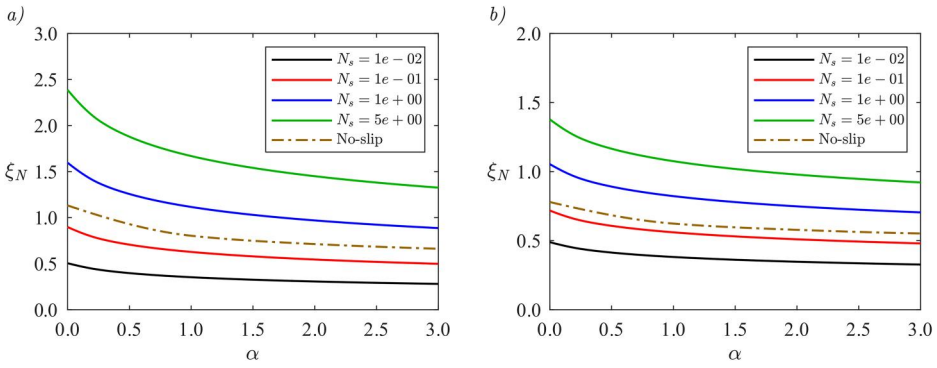

FIG. 4. Similarity coefficient at the current front ($X = X_N$) for (a) planar geometry and (b) axisymmetric geometry. Solid lines show the behavior of ξ_N for different values of the slip number N_s, as given by Eq. (22), while dashed lines correspond to the classical no-slip value defined by Eq. (15).

$$X_N = \xi_N T^{\frac{3\alpha+1}{5+3d}}, \tag{27}$$

$$X_N' = \xi_N' T^{\frac{2\alpha+1}{4+2d}}, \tag{28}$$

for the no-slip and very-slippery regimes, respectively. By combining these expressions with Eqs. (15) and (22), one can identify the temporal ranges over which the very-slippery front propagates farther than that predicted by the no-slip theory. The two propagation exponents coincide for $\alpha = 1/2$ in planar geometry ($d = 0$) and for $\alpha = 1$ in axisymmetric geometry ($d = 1$). Nevertheless, the comparison also depends on the magnitude of the prefactors ξ_N and ξ_N'. Figure 4 shows the dependence of the similarity coefficient at the front on the injection exponent α and the slip number N_s. As N_s increases, the value of ξ_N' in the very-slippery limit also increases, in agreement with the scaling predicted by Eq. (22). We note that the no-slip similarity coefficient ξ_N becomes smaller than the corresponding very-slippery value ξ_N' when $N_s \gtrsim 0.3$ or $N_s \gtrsim 0.2$, in plane or radial geometry, respectively. In the planar case, the relative position of the two fronts is determined by

$$T \lessgtr \left(\frac{\xi_N'}{\xi_N}\right)^{\frac{20}{2\alpha-1}} \quad \text{for} \quad \alpha \gtrless 1/2, \tag{29}$$

where the very-slippery front propagates farther than the no-slip front for times satisfying the corresponding inequality. Similarly, in axisymmetric geometry, the very-slippery front overtakes the no-slip front when

$$T \lessgtr \left(\frac{\xi_N'}{\xi_N}\right)^{\frac{24}{\alpha-1}} \quad \text{for} \quad \alpha \gtrless 1. \tag{30}$$

As an illustrative example, consider planar geometry with $\alpha = 1$. In this case, the very slippery solution predicts a faster front only for times $T < (\xi_N'/\xi_N)^{20} \approx 7 \times 10^{-8}$ when $N_s = 0.01$, implying that for all practical purposes, the no-slip solution always propagates faster. Conversely, for $\alpha = 0$, the very-slippery solution would overtake the no-slip one only at extremely long times, namely, for $T > (\xi_N'/\xi_N)^{20} \approx 10^7$. These nondimensional time intervals broaden significantly as the slip number increases. For instance, when $N_s = 1$, the corresponding thresholds become $T < 718$ for $\alpha = 1$ and $T > 0.01$ for $\alpha = 0$. The dependence of these crossover times on α and N_s is summarized in Fig. 5, where the limiting time T_{lim}, at which the two asymptotic solutions predict the same front position, is plotted as a function of α for different values of the slip number. The figure highlights that N_s strongly influences the temporal window over which the very-slippery front propagates ahead of the no-slip one. Specifically, this regime corresponds to the region below (above) the T_{lim} curve for $\alpha > 1/2$ ($\alpha < 1/2$) in planar geometry and for $\alpha > 1$ ($\alpha < 1$) in axisymmetric geometry.

IV. FULL NUMERICAL RESULTS

This section presents a numerical procedure to solve the partial differential problem defined by Eqs. (10) and (11) using an explicit time-integration scheme. A second-order Runge–Kutta method, implemented within a predictor–corrector framework, was developed in MATLAB®. The governing variables are discretized on a uniform spatial grid, with primary variables defined at grid nodes and spatial derivatives evaluated at staggered midpoints. For $\alpha > 0$, the initial condition for the dimensionless current thickness is prescribed as

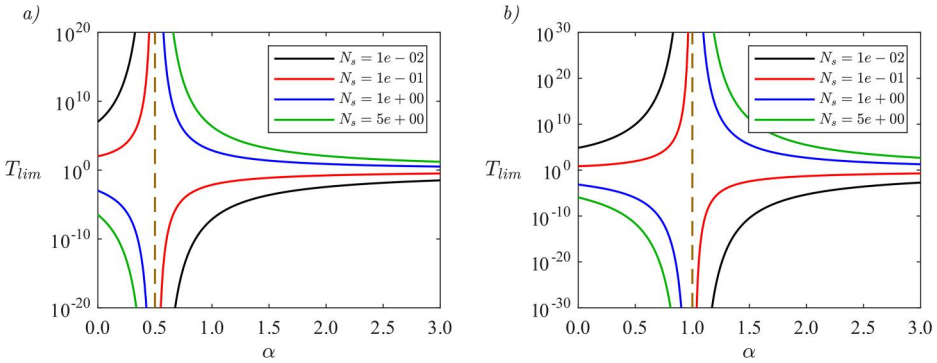

FIG. 5. Similarity front propagation. The curves represent Eqs. (29) and (30) for different values of the slip number N_s in (a) planar and (b) axisymmetric geometries, respectively, and identify the nondimensional time T_{lim} at which the very-slippery and no-slip front positions coincide. The very-slippery solution predicts a farther front position for $T \lessgtr T_{\text{lim}}$ when $\alpha \gtrless 1/2$ in planar geometry and $\alpha \gtrless 1$ in axisymmetric geometry.

$$H(X,0) = H_{in}\left(\frac{X_{N0} - X}{X_{N0}}\right)^{E} \quad \text{for} \quad \Delta X < X < X_{N0}, \tag{31}$$

where H_{in} and E are the dimensionless constants, and X_{N0} denotes the initial position of the current front.

The boundary condition at the origin is expressed in terms of the imposed inflow rate as

$$(2\pi)^d X^d H(0,T) U(0,T) = \alpha T^{\alpha-1}, \tag{32}$$

which is obtained by differentiating the global mass conservation relation (11) with respect to T, and the expression of the dimensionless horizontal velocity U can be easily derived from Eqs. (5) and (10). To ensure the stability and convergence of the explicit scheme, the parameters H_{in} and E were selected so that Eq. (31) approximately satisfies the discretized version of Eq. (32). The other boundary condition is simply given by imposing the constraint $H(X_N, T) = 0$ at the current front. The spatial grid spacing ΔX and time step ΔT were also adjusted according to the values of the injection exponent α and the slip number N_s. In most simulations, we employed $\Delta X = 0.05$ and an initial time step of $\Delta T = 10^{-6}$.

The integration scheme was first validated against the classical no-slip solution (14) by imposing the condition $N_s = 0$ within the numerical code. Results are presented in Fig. 6, showing the overlapping between the two solutions even for $T = 0.1$ in the case of a constant fluid injection ($\alpha = 1$), whereas for the dam-break release ($\alpha = 0$), the numerical scheme perfectly reproduces the no-slip solution from $T = 1$ onward. Grid sensitivity tests were also performed to ensure that grid spacing does not affect the convergence of the numerical scheme to the asymptotic solution.

Figure 7 show the gravity current profiles for an instantaneous fluid release ($\alpha = 0$) under low- and high-slip number conditions, corresponding to $N_s = 0.001$ and $N_s = 0.1$. The results obtained from the full numerical integration are compared with the similarity solutions derived in the no-slip and very-slippery asymptotic limits. For $N_s = 0.001$, the effect of basal sliding is almost negligible, and the no-slip similarity solution provides an accurate approximation of the numerical profiles even at long times. This behavior is expected, since the very-slippery similarity solution relies on the assumption $H \ll N_s$, which is satisfied only after the current has propagated over sufficiently large distances and thinned considerably. The opposite behavior is observed when a more slippery scenario is considered, namely, for $N_s = 0.1$. In this case, the condition $H \ll N_s$ is satisfied at earlier times and over shorter propagation distances, so that the very-slippery similarity solution progressively converges toward the full numerical profile and provides a more accurate prediction of the front position than the no-slip solution at long times. In axisymmetric geometry, the gravity current spreads over an increasing volume, which promotes faster thinning of the current. As a result, the very-slippery condition of validity is reached at shorter distances than in the planar case, and the similarity solution becomes essentially indistinguishable from the full numerical profile by $T = 10^5$.

Figure 8 present the corresponding results for a constant-flux injection ($\alpha = 1$). In this case, the very-slippery similarity solution is unable to capture the actual dynamics of the gravity current when the slip number N_s is small, whereas the no-slip similarity solution progressively approaches the full-numerical profile, with a velocity that is dependent on the N_s value: the higher the slip number, the larger the slip contribution; thus, the longer the time needed for the no-slip

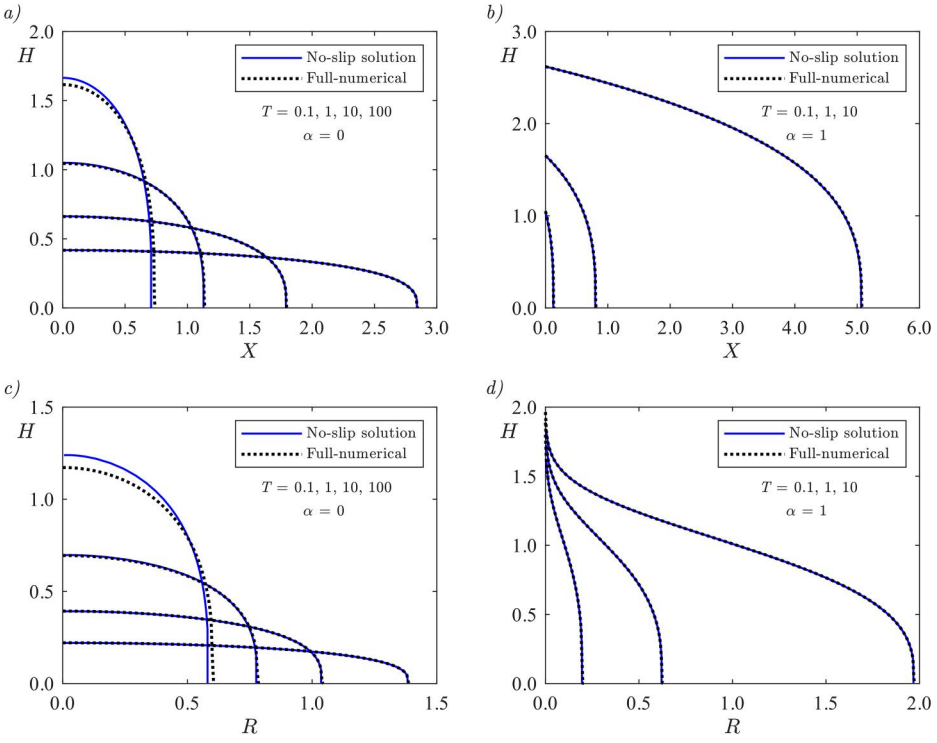

FIG. 6. Validation of the full-numerical scheme. Blue curves represent the solution of the no-slip ODE (14) while black dashed lines result from the direct integration of the PDE (10).

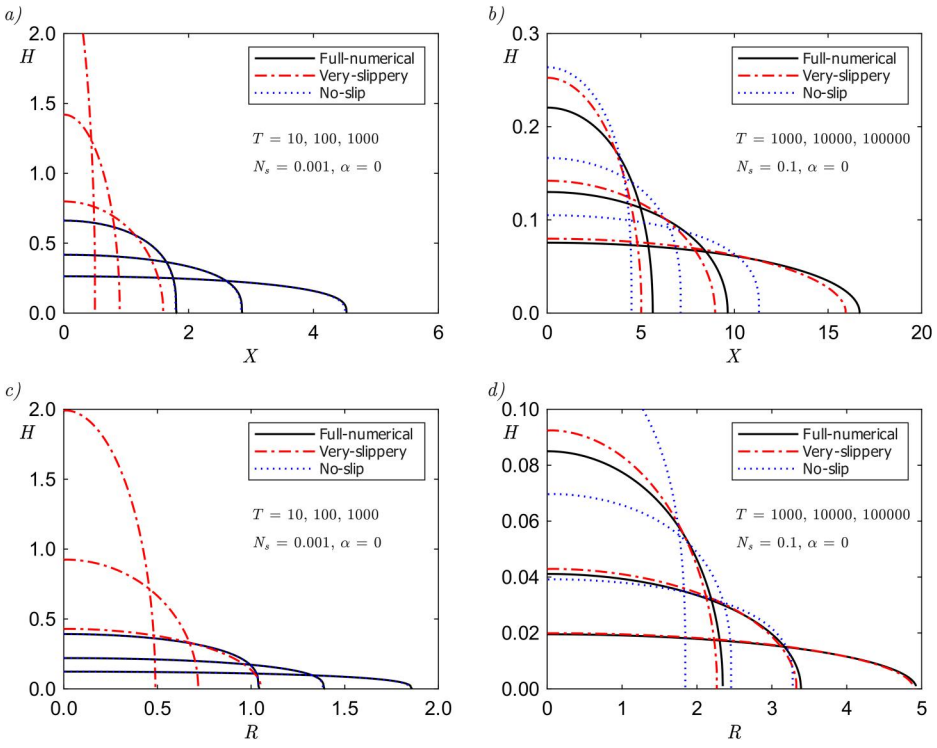

FIG. 7. Comparison between fully numerical solutions and very-slippery and no-slip similarity solutions for $\alpha = 0$ and $N_s = 0.001; 0.1$. Panels (a) and (b) and (c) and (d) correspond to planar and axisymmetric coordinates, respectively.

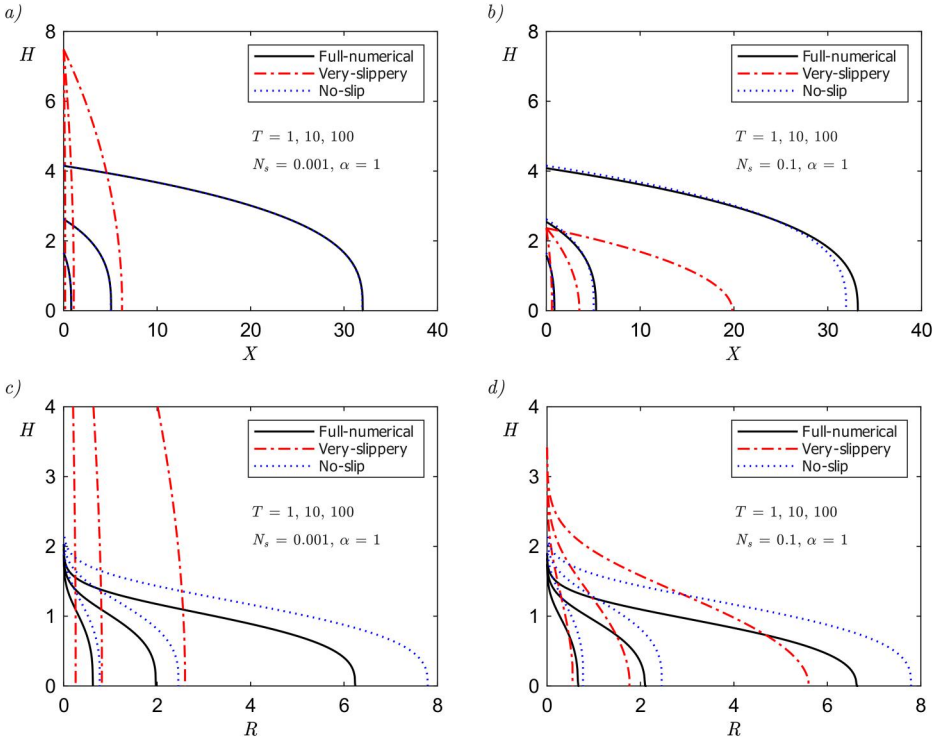

FIG. 8. Comparison between full numerical solutions and very-slippery and no-slip similarity solutions for $\alpha = 1$ and $N_s = 0.001; 0.1$. Panels (a) and (b) and (c) and (d) correspond to planar and axisymmetric coordinates, respectively.

regime to become representative of the real spreading of the current. This behavior also indicates that basal slip plays a significant role primarily when low injection rates or small injection volumes are considered, unless macroscopic slip lengths are involved, as discussed in Sec. V. Finally, it is also evident that the gravity current requires longer times to reach its asymptotic regime in planar geometry than in axisymmetric geometry, reflecting the enhanced thinning associated with radial spreading.

V. A DIMENSIONAL EXAMPLE

In Secs. III and IV, we compared different solution approaches and slip regimes using nondimensional variables. Here, we present a dimensional example illustrating the spreading of a gravity current which properties are representative of the fluid (golden syrup) employed by Yan and Kowal[11] (see Table I of their work). In their experiments, they were able to generate a macroscopic slip length on the order of $\overline{k} \approx 1\,\text{cm}$, which is significantly larger than typical slip lengths that can be found in the literature, as discussed in Appendix A. Table I summarizes fluid properties, slip characteristics, and injection conditions we employed to develop our numerical example. Such high value of $\overline{k}$ results in slip numbers larger than unity even for non-micro injection volumes, which are otherwise needed to spot observable effects of basal sliding for microscopic values of $\overline{k}$.

Figures 9(a) and 9(c) show the propagation of the fluid injected at a constant rate in planar and axisymmetric geometries. In the planar case, as expected, the very-slippery similarity solution is representative of the actual spreading dynamics at small times after injection starts: as the current propagates, its height increases; thus, the full-numerical profile gradually detaches from the very-slippery limit. However, this requires quite a long time due to the high value of the slip number N_s; thus, the no-slip asymptotic is far away from being reached after 3 min. The axisymmetric case shows, instead, a perfect overlapping between the full-numerical solution and the very-slippery limit, which is expected as the no-slip assumption $h \gg \overline{k} = 1\,\text{cm}$ will never be respected, since in this case the average current height remains constant over time, as already shown in Fig. 3.

Figures 9(b) and 9(d) show the corresponding profiles for a linearly increasing injection of fluid ($\alpha = 2$). In plane coordinates, the

TABLE I. Injection and slip parameters of a fluid which properties resemble those of Yan and Kowal[11] experiments.

Geometry	α	$\overline{k}$ (m)	ρ (kg m^{-3})	ν (cm^2 s^{-1})	Q (m^{d+2} s$^{-\alpha}$)	N_s
Planar ($d = 0$)	1	0.01	1430	100	10^{-4}	2.14
Planar ($d = 0$)	2	0.01	1430	200	10^{-4}	2.21
Axisymmetric ($d = 1$)	1	0.01	1430	100	10^{-6}	1.77
Axisymmetric ($d = 1$)	2	0.01	1430	200	10^{-6}	1.89

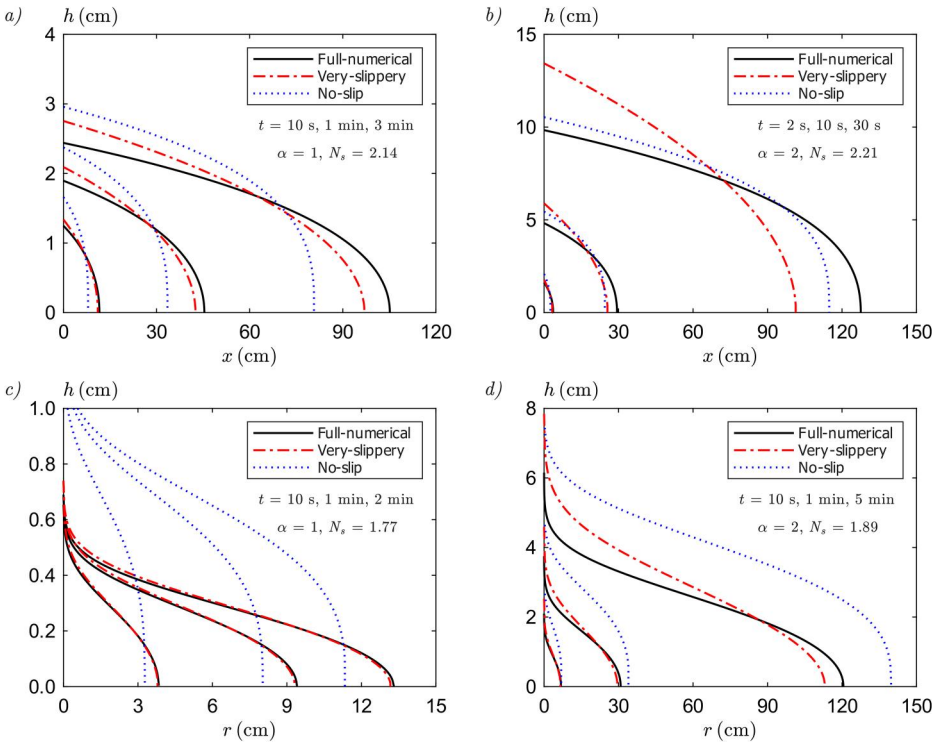

FIG. 9. Full numerical and similarity profiles for constant injection (left column) and linearly increasing injection (right column) of the fluid described in Table I over a slippery substrate in (a) and (b) planar and (c) and (d) axisymmetric geometries.

validity condition for the very-slippery regime $h \ll \bar{k}$ is more rapidly violated during the evolution with respect to the $\alpha = 1$ case, as the GC height increases much faster for $\alpha = 2$. Hence, the very-slippery solution is not representative of the actual propagation of the GC already after $t = 10$ s, and the current approaches the no-slip limit at a faster rate. In the axisymmetric case, since the injected volume spreads over a larger surface area, the gravity current front propagates over shorter distances than in planar geometry; thus, much longer times are needed to observe an analogous behavior.

These considerations are also highlighted in Fig. 10, which shows the evolution of the GC front predicted by the three solutions for $\alpha = 2$ in both plane and radial coordinates. It is again evident that the full-numerical profile needs much shorter times to reach the no-slip

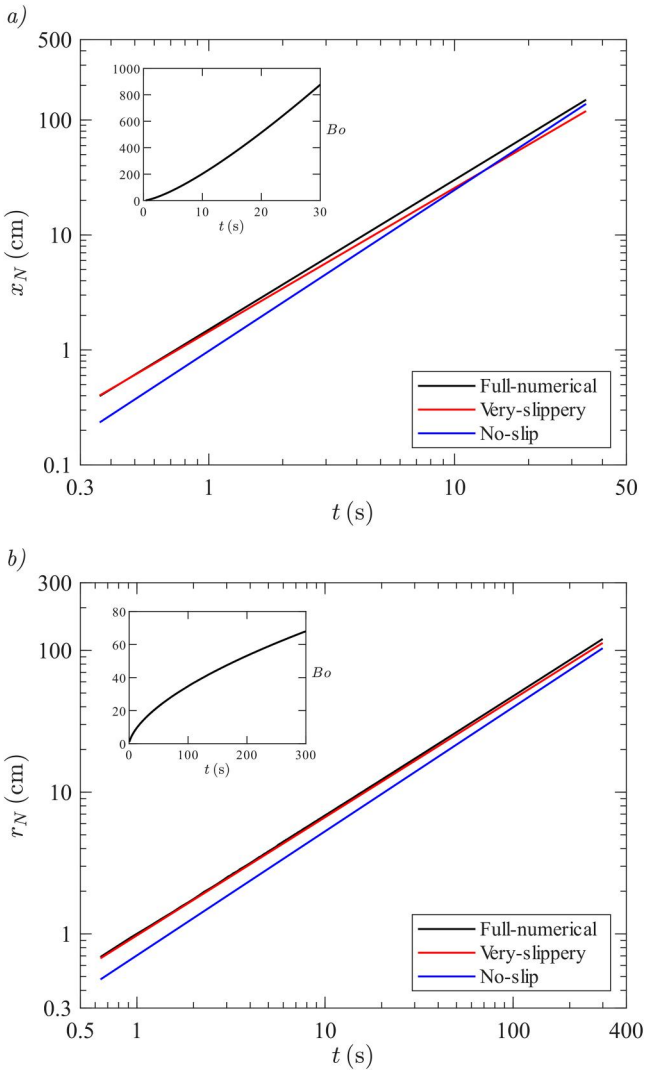

FIG. 10. Current front position for linearly increasing injection ($\alpha = 2$) of the fluid described in Table I in (a) planar and (b) axisymmetric geometries. Subplots show the temporal evolution of the Bond number $Bo\,(t) = \rho g \bar{h}^2/\sigma$, being $\bar{h} = \bar{h}\,(t)$ as the average thickness of the GC.

asymptotic in planar geometry with respect to the axisymmetric case. The plots also show the evolution of the Bond number $Bo = \rho g L^2/\sigma$ over time, which is computed by taking the average height of the current,

$$\bar{h} = x_0 \cdot \frac{2^d}{X_N^{d+1}} \int_0^{X_N} X^d H \mathrm{d}X, \tag{33}$$

as the characteristic length L. The surface tension corresponds to that of golden syrup, equal to $\sigma = 0.08\,\mathrm{N/m}$.[18] Again, in the planar case, the condition $Bo \gg 1$ becomes rapidly satisfied due to the smaller area on which the current propagates, assuming values of $Bo \approx 100$ already after $t = 5$ s, whereas larger time horizons are needed in the axisymmetric case due to the slower increase in the current height. This justifies the assumption of negligible capillary forces beyond a time threshold and the description of our flow case as a GC flow problem. The lubrication theory condition $h/l \ll 1$ is also respected, as the ratio $\bar{h}/x_N$ gradually decreases over time, thus validating the starting assumption of negligible extensional stresses with respect to shear stresses. We also note that experiment C of Yan and Kowal,[11] which they suspected of potentially relevant contributions of extensional stresses in the very-slippery limit, employed a much more viscous fluid ($\nu = 323.2\,\mathrm{m^2/s}$) with respect to those we selected for our numerical simulations, thus confirming that the effect of such stresses would be negligible within our case.

VI. SUMMARY AND CONCLUSIONS

We investigated the free-surface propagation of a Newtonian gravity current over a slippery substrate, accounting for basal slip through a nonzero velocity u_s at the base of the current. This velocity is assumed to obey a linear (Navier) slip law and is proportional to the slip length $\bar{k}$. We derived similarity solutions describing the spreading of the gravity current in both planar and axisymmetric geometries under two opposite asymptotic regimes: a no-slip limit ($H \gg N_s$) and a very-slippery limit ($H \ll N_s$).

In the no-slip regime, the resulting self-similar solutions reduce to the classical results available in the literature. In contrast, we obtained new similarity solutions characterizing the propagation of gravity currents in the very-slippery limit. To bridge these two asymptotic behaviors, we developed a fully numerical scheme capable of resolving the transient regime connecting them. Our theoretical analysis and numerical results show that the duration of this transitional regime increases markedly as the slip number N_s decreases.

The slip number N_s may or may not explicitly appear in the governing partial differential equation depending on the choice of nondimensionalization scales, as discussed in Appendix B. Within the nondimensionalization adopted in this work, we showed that decreasing values of N_s narrow the temporal interval over which the very-slippery solution reproduces the full numerical results, regarded as the most complete representation of the flow since they account for both no-slip and slip-induced contributions in the governing equation.

The relevance of the very-slippery regime also depends on the injection protocol. For an instantaneous release ($\alpha = 0$), the gravity current progressively thins as it spreads, so that the condition $H \ll N_s$ may eventually be approached at sufficiently long times. In contrast, constant-flux injections ($\alpha = 1$) or linearly increasing flow rates ($\alpha = 2$) produce gravity currents whose thickness remains

constant or increases in time, implying that the very-slippery limit can be relevant only during the early stages of the flow, and only for sufficiently large values of N_s.

However, as discussed in Appendix A, typical values of the slip length are on the order of tens to hundreds of nanometers. Therefore, for such fluids, we expect to observe sensible effects of basal sliding only for micro-scale gravity currents, as low-injection volumes would result in sufficiently large slip numbers, on the order of $N_s \approx 0.1$, leading to a substantial modification of the gravity current spreading.

The study of micro-scale gravity currents would involve non-negligible capillary forces and is left for future studies. Instead, we presented a dimensional example describing the spreading of a gravity current with similar features to the one employed in Yan and Kowal[11] experiments, considering both constant-flux and linearly increasing injection in planar and axisymmetric geometries. Their experimental setup resulted in macroscopic slip lengths, corresponding to values of N_s greater than unity even for non-micro injection volumes. In dimensional terms, the very-slippery condition here requires $h \ll \overline{k} = 1\,\text{cm}$, and this inequality can be satisfied only over short times for constant-flux injection ($\alpha = 1$) and for even smaller intervals for a linearly increasing flow rate ($\alpha = 2$). However, this is strictly dependent on the geometry of the problem, since the axisymmetric case requires the GC to propagate over a larger surface, i.e., higher times are needed for the transition from the very-slippery to the no-slip asymptotic solution with respect to the planar case.

We have shown that the presence of basal sliding plays a significant role over the time scales typically accessible after injection when either micro-gravity currents or high slippery substrates are considered. In contrast, for large-scale gravity currents—such as glaciers—much longer evolution times would be required for basal sliding to produce appreciable effects on the propagation dynamics. Such long-term phenomena are, therefore, beyond the scope of the present study. Nevertheless, the influence of basal slip on gravity current dynamics depends sensitively on the fluid properties, the injection protocol, and the slip length—and thus, on the characteristics of the substrate over which the current propagates—leading to a wide range of possible behaviors. This variability suggests that a more comprehensive understanding and modeling of basal sliding could further improve predictions of gravity current propagation.

Future work may proceed along several directions. First, alternative slip laws—such as higher-order or nonlinear formulations—could be explored, as the Navier slip condition adopted here represents the simplest description of basal sliding and more elaborate models may better capture the underlying physical mechanisms. Second, carefully designed laboratory experiments are needed to assess the predictive capability of the proposed theoretical framework and to quantify slip effects under controlled conditions, despite the inherent challenges associated with reproducing basal sliding in experimental settings. Finally, for large-scale slippery substrates, such as subglacial tills beneath glaciers, additional physical processes should be incorporated into the model formulation, including thermodynamic effects, and substantially longer simulation times would be required to capture the impact of basal sliding on the evolution of the overlying flow.

ACKNOWLEDGMENTS

Bruno Rossi was supported by the Università di Bologna through the doctoral scholarship "Free-surface flow in heterogeneous porous media" (PhD@DICAM, Call 2025). Vittorio Di Federico was supported by the Università di Bologna under the Ricerca Fondamentale Orientata (RFO) 2023 program.

AUTHOR DECLARATIONS

Conflict of Interest

The authors have no conflicts to disclose.

Author Contributions

Bruno Rossi: Conceptualization (equal); Data curation (lead); Formal analysis (lead); Investigation (lead); Methodology (lead); Software (lead); Validation (lead); Visualization (lead); Writing – original draft (lead). **Vittorio Di Federico:** Conceptualization (equal); Funding acquisition (equal); Project administration (equal); Resources (equal); Supervision (equal); Writing – review & editing (equal).

DATA AVAILABILITY

The data that support the findings of this study are available within the article.

APPENDIX A: VALUES OF THE SLIP NUMBER N_s

The nondimensionalization introduced in Eq. (9) leads to the governing equation (10) depending explicitly on the slip number N_s, defined as follows:

$$N_s = \frac{\overline{k}}{x_0} = \overline{k}\left[Q\left(\frac{\nu}{g}\right)^{\alpha}\right]^{-\frac{1}{\alpha+(d+2)}}, \tag{A1}$$

which combines fluid properties (through ν), injection characteristics (through Q and α), geometry (through d), and the slip length $\overline{k}$. The slip number does not explicitly appear when the nondimensionalization proposed by Yan and Kowal[11] is adopted, since in that case the height scale is chosen equal to the slip length. As discussed in Appendix B, the present definition of N_s can be interpreted as the ratio between their height scale, $h_0' = \overline{k}$, and the characteristic length scale adopted here, $h_0 = x_0$.

The explicit presence of N_s in the governing equations modulates the relative importance of the slip-induced contribution with respect to the classical no-slip term. In this Appendix, we report representative values of the slip number computed from literature measurements of the slip length $\overline{k}$ for various fluids. These values are listed in Table II for both planar and axisymmetric nondimensionalizations. The slip lengths reported therein originate from laboratory experiments in which the substrates are typically coated with hydrophobic organic compounds, such as trimethylchlorosilane (TMS), octadecyltrichlorosilane (OTS), or hexadecyltrichlorosilane (HTS).

Equation (A1) shows that larger values of N_s and, thus, stronger relative effects of basal sliding, are obtained for smaller injected volumes or fluxes, i.e., for micro-scale gravity currents characterized by very small values of Q. This explains why the table focuses on small injection volumes, for which slip effects become potentially observable over the relatively short time scales following

TABLE II. Estimated ranges of the slip number N_s for planar ($d = 0$) and radial ($d = 1$) geometry based on literature slip-length values.

Fluid	Surface	ν ($m^2\,s^{-1}$)	α ($m^2\,s^{-\alpha}$)	Q	$\bar{k}$ (m)	$N_s\,(d=0)$	$N_s\,(d=1)$	Source
Glycerol (20 °C)	Glass + OTS	1.12×10^{-3}	0	10^{-9}	2.0×10^{-7}	6.32×10^{-3}	2.00×10^{-4}	Cottin-Bizonne *et al.*[19]
			1			4.12×10^{-3}	3.44×10^{-4}	
			2			3.33×10^{-3}	4.76×10^{-4}	
Mercury (20 °C)	Quartz + TMS	1.14×10^{-7}	0	10^{-9}	7.0×10^{-8}	2.21×10^{-3}	7.00×10^{-5}	Churaev *et al.*[20]
			1			3.09×10^{-2}	1.20×10^{-3}	
			2			1.15×10^{-1}	6.59×10^{-3}	
1-Decane (25 °C)	Iron	1.22×10^{-4}	0	10^{-9}	4.2×10^{-8}	1.33×10^{-3}	4.20×10^{-5}	Mehrnia and Pelz[21]
			1			1.81×10^{-3}	1.26×10^{-4}	
			2			2.12×10^{-3}	2.43×10^{-4}	
Hexadecane (25 °C)	Glass	3.94×10^{-6}	0	10^{-9}	3.0×10^{-8}	9.49×10^{-4}	3.00×10^{-5}	Cheng and Giordano[22]
			1			4.07×10^{-3}	2.12×10^{-4}	
			2			8.42×10^{-3}	6.85×10^{-4}	
Benzene (25 °C)	Borosilicate + HTS	6.89×10^{-7}	0	10^{-9}	5.0×10^{-8}	1.58×10^{-3}	5.00×10^{-5}	Cho *et al.*[23]
			1			1.21×10^{-2}	5.46×10^{-4}	
			2			3.35×10^{-2}	2.29×10^{-3}	

injection. Finally, we note that increasing the injection exponent α generally leads to higher values of the slip number.

However, for such fluids, N_s rarely exceeds the threshold value $N_s \approx 0.1$, which can, therefore, be regarded as an upper bound representative of a high-slip regime. To generate macroscopic slip lengths, and therefore, much larger N_s values, specific laboratory settings must be arranged, as the one proposed by Yan and Kowal,[11] whose slip length was on the order of $\bar{k} \approx 1$ cm.

APPENDIX B: AN ALTERNATIVE NON-DIMENSIONALIZATION

In Sec. II, the governing problem defined by Eqs. (6) and (7) was nondimensionalized using the characteristic length and time scales introduced in Eq. (9), following the approach of Lister.[17] This choice yields a formulation that is valid for any injection exponent $\alpha \geq 0$ but retains an explicit dependence on the slip number N_s in the nondimensional problems (10) and (11).

An alternative nondimensionalization was proposed by Yan and Kowal[11] for planar geometry ($d = 0$) and constant-flux injection ($\alpha = 1$), in which the slip length is used as the characteristic vertical scale. Extending their approach to both planar and axisymmetric geometries and to a generic injection exponent α leads to the following choices for the characteristic height, length, and time scales:

$$h_0' = \bar{k}; \quad x_0' = \left(\left(\frac{g}{\nu}\right)^{\alpha} \frac{\bar{k}^{3\alpha+1}}{Q}\right)^{\frac{1}{2\alpha-(d+1)}}; \quad t_0' = \left(\frac{g}{\nu}\frac{\bar{k}^{5-d}}{Q^{2-d}}\right)^{\frac{1}{(2-d)\alpha-1}}. \tag{B1}$$

Upon introducing the characteristic scales defined in Eq. (B1) into Eqs. (6) and (7), the governing problem reduces to

$$\frac{\partial H}{\partial T} = \frac{1}{X^d}\frac{\partial}{\partial X}\left(\frac{1}{3}X^d H^3 \frac{\partial H}{\partial X} + X^d H^2 \frac{\partial H}{\partial X}\right), \tag{B2}$$

together with the global mass conservation constraint and front condition

$$(2\pi)^d \int_0^{X_N} X^d H \, dX = T^{\alpha}; \quad H(X_N, T) = 0. \tag{B3}$$

This alternative nondimensionalization yields a governing equation that is formally independent of the fluid properties and slip length. However, its range of validity is restricted by the definition of the characteristic scales: specifically, the scaling breaks down for $\alpha = 1/2$ in planar geometry ($d = 0$) and for $\alpha = 1$ in axisymmetric geometry ($d = 1$), for which the exponents in Eq. (B1) become singular.

For values of α such that the alternative nondimensionalization is well defined—namely, $\alpha \neq 1/2$ in planar geometry and $\alpha \neq 1$ in axisymmetric geometry—it follows directly from Eq. (20) that similarity solutions of the differential problem (B2) and (B3) in the very-slippery limit can be obtained by introducing the scalings

$$\xi = XT^{-\frac{2\alpha+1}{4+2d}}; \quad H = \xi_N T^{\frac{(2-d)\alpha-1}{4-d}}\Phi(\zeta), \tag{B4}$$

where $\zeta = \xi/\xi_N$. Substitution of these expressions into the governing equations yields

$$\frac{d}{d\zeta}\left[\zeta^d \Phi^2 \frac{d\Phi}{d\zeta}\right] + \left(\frac{2\alpha+1}{4+2d}\right)\zeta^{d+1}\frac{d\Phi}{d\zeta} - \left(\frac{(2-d)\alpha-1}{4-d}\right)\zeta^d\Phi = 0, \tag{B5}$$

together with the normalization condition and front boundary condition as follows:

$$\xi_N = [(2\pi)^d \int_0^1 \zeta^d \Phi(\zeta) d\zeta]^{-\frac{1}{2+d}}; \quad \Phi(1) = 0, \tag{B6}$$

while the similarity scalings and resulting solution in the no-slip limit coincide exactly with those obtained using the nondimensionalization adopted in the main text, since the slip-induced term is neglected in both formulations.

The main drawback of this alternative nondimensionalization lies in the lack of universality of the no-slip and very-slippery similarity solutions at critical values of the injection exponent α. In particular, for these values, the characteristic scales become singular, and the corresponding similarity structure must be treated separately.

As an example, consider axisymmetric geometry and constant-flux injection ($\alpha = 1$). In this case, the problem must be reformulated by introducing an arbitrary time scale $\tilde{t}_0$, from which the characteristic radial scale is defined as $\tilde{r_0}^2 = \frac{Q\tilde{t}_0}{\bar{k}}$ and the governing equations (B2) and (B3) reduce to

$$\frac{\partial \tilde{H}}{\partial \tilde{T}} = \frac{\Lambda_R}{\tilde{R}} \frac{\partial}{\partial \tilde{R}} \left(\frac{1}{3} \tilde{R} \tilde{H}^3 \frac{\partial \tilde{H}}{\partial \tilde{R}} + \tilde{R} \tilde{H}^2 \frac{\partial \tilde{H}}{\partial \tilde{R}} \right); \quad \Lambda_R = \frac{g\bar{k}^4}{\nu Q}, \tag{B7}$$

$$2\pi \int_0^{\tilde{R}_N} \tilde{R} \tilde{H} \, d\tilde{R} = \tilde{T}. \tag{B8}$$

To solve this differential problem in the no-slip limit, we introduce the similarity scalings as follows:

$$\tilde{\xi} = \tilde{R} \tilde{T}^{-\frac{1}{2}}; \quad \tilde{H} = \tilde{\xi_N}^{2/3} \tilde{\Phi}(\tilde{\zeta}); \quad \tilde{\zeta} = \tilde{\xi}/\tilde{\xi_N}, \tag{B9}$$

which reduce the governing equations to

$$\Lambda_R \frac{d}{d\tilde{\zeta}} \left[\frac{1}{3} \tilde{\zeta} \tilde{\Phi}^3 \frac{d\tilde{\Phi}}{d\tilde{\zeta}} \right] + \frac{1}{2} \tilde{\zeta}^2 \frac{d\tilde{\Phi}}{d\tilde{\zeta}} = 0, \tag{B10}$$

$$\tilde{\xi_N} = \left[2\pi \int_0^1 \tilde{\zeta} \tilde{\Phi}(\tilde{\zeta}) d\tilde{\zeta} \right]^{-3/8}. \tag{B11}$$

The very-slippery limit can be treated by introducing the following self-similar transformation:

$$\tilde{\xi} = \tilde{R} \tilde{T}^{-\frac{1}{2}}; \quad \tilde{H} = \tilde{\xi_N} \tilde{\Phi}(\tilde{\zeta}); \quad \tilde{\zeta} = \tilde{\xi}/\tilde{\xi_N}, \tag{B12}$$

which allows Eqs. (B7) and (B8) to be recast as

$$\Lambda_R \frac{d}{d\tilde{\zeta}} \left[\tilde{\zeta} \tilde{\Phi}^2 \frac{d\tilde{\Phi}}{d\tilde{\zeta}} \right] + \frac{1}{2} \tilde{\zeta}^2 \frac{d\tilde{\Phi}}{d\tilde{\zeta}} = 0, \tag{B13}$$

$$\tilde{\xi_N} = [2\pi \int_0^1 \tilde{\zeta} \tilde{\Phi}(\tilde{\zeta}) d\tilde{\zeta}]^{-1/3}. \tag{B14}$$

A Frobenius expansion of $\tilde{\Phi}$ near the current front in the very-slippery limit yields the following approximate expression:

$$\tilde{\Phi}(\tilde{\zeta}) = \frac{1}{\Lambda_R^{1/2}} (1 - \tilde{\zeta})^{1/2} \left[1 + \frac{1}{12} (1 - \tilde{\zeta}) \right]. \tag{B15}$$

Analogously, for planar geometry ($d = 0$), the critical case $\alpha = 1/2$ can be nondimensionalized by introducing the characteristic length and velocity scales $\tilde{x_0} = \frac{Q\sqrt{\tilde{t}_0}}{\bar{k}}$ and $\tilde{u_0} = \tilde{x_0}/\tilde{t_0}$, where $\tilde{t_0}$ is again an arbitrary time scale. With these definitions, the governing problem (B2) and (B3) can be recast in the following form:

$$\frac{\partial \tilde{H}}{\partial \tilde{T}} = \Lambda_P \frac{\partial}{\partial \tilde{X}} \left(\frac{1}{3} \tilde{H}^3 \frac{\partial \tilde{H}}{\partial \tilde{X}} + \tilde{H}^2 \frac{\partial \tilde{H}}{\partial \tilde{X}} \right); \quad \Lambda_P = \frac{g\bar{k}^5}{\nu Q^2}, \tag{B16}$$

$$\int_0^{\tilde{X}_N} \tilde{H} \, d\tilde{X} = \tilde{T}^{1/2}. \tag{B17}$$

To determine similarity solutions to (B16) and (B17) in the no-slip limit, we introduce the similarity scalings

$$\tilde{\xi} = \tilde{X} \tilde{T}^{-\frac{1}{2}}; \quad \tilde{H} = \tilde{\xi_N}^{2/3} \tilde{\Phi}(\tilde{\zeta}); \quad \tilde{\zeta} = \tilde{\xi}/\tilde{\xi_N}, \tag{B18}$$

which reduce the governing equations to

$$\Lambda_P \frac{d}{d\tilde{\zeta}} \left[\frac{1}{3} \tilde{\Phi}^3 \frac{d\tilde{\Phi}}{d\tilde{\zeta}} \right] + \frac{1}{2} \tilde{\zeta} \frac{d\tilde{\Phi}}{d\tilde{\zeta}} = 0, \tag{B19}$$

$$\tilde{\xi_N} = \left[\int_0^1 \tilde{\Phi}(\tilde{\zeta}) d\tilde{\zeta} \right]^{-3/5}. \tag{B20}$$

The similarity solution in the very-slippery limit is obtained by introducing the scalings

$$\tilde{\xi} = \tilde{X} \tilde{T}^{-\frac{1}{2}}; \quad \tilde{H} = \tilde{\xi_N} \tilde{\Phi}(\tilde{\zeta}); \quad \tilde{\zeta} = \tilde{\xi}/\tilde{\xi_N}, \tag{B21}$$

which allow Eqs. (B16) and (B17) to be recast as

$$\Lambda_P \frac{d}{d\tilde{\zeta}} \left[\tilde{\Phi}^2 \frac{d\tilde{\Phi}}{d\tilde{\zeta}} \right] + \frac{1}{2} \tilde{\zeta} \frac{d\tilde{\Phi}}{d\tilde{\zeta}} = 0, \tag{B22}$$

$$\tilde{\xi_N} = \left[\int_0^1 \tilde{\Phi}(\tilde{\zeta}) d\tilde{\zeta} \right]^{-1/2}. \tag{B23}$$

A Frobenius expansion of $\tilde{\Phi}$ near the current front in the very-slippery limit yields the approximate expression

$$\tilde{\Phi}(\tilde{\zeta}) = \frac{1}{\Lambda_P^{1/2}} (1 - \tilde{\zeta})^{1/2} \left[1 - \frac{1}{12} (1 - \tilde{\zeta}) \right]. \tag{B24}$$

We note that this alternative nondimensionalization leads to the very-slippery and no-slip asymptotic regimes being characterized by the conditions $H \ll 1$ and $H \gg 1$, respectively. As a consequence, when expressed in nondimensional variables, the temporal validity of these regimes is independent of the slip number N_s, in contrast with the formulation adopted in the main text, where N_s explicitly controls the transition between regimes. However, when the solutions are interpreted in dimensional terms, both nondimensionalizations yield the same physical conditions for the applicability of the asymptotic limits, namely, $h \ll \bar{k}$ for the very-slippery regime and $h \gg \bar{k}$ for the no-slip regime. These inequalities must, therefore, be satisfied for the semi-analytical solutions to accurately describe the actual spreading dynamics of the gravity current.

REFERENCES

[1] J. E. Simpson, *Gravity Currents: In the Environment and the Laboratory* (Cambridge University Press, 1999).
[2] T. Sokolov and T. Zemach, "The effects of vegetation on gravity currents propagating in channels of general cross-sections," Phys. Fluids **37**, 113120 (2025).
[3] M. Maggi, G. Di Lollo, and C. Adduce, "Dynamics and mixing of gravity currents over an array of cylindrical obstacles," Phys. Fluids **37**, 076629 (2025).
[4] V. Di Federico, S. Malavasi, and S. Cintoli, "Viscous spreading of non-Newtonian gravity currents on a plane," Meccanica **41**, 207–217 (2006).
[5] T. Moodie, "Gravity currents," J. Comput. Appl. Math. **144**, 49–83 (2002).
[6] S. Longo, "Gravity currents of viscous fluids in a vertically widening and converging fracture," Phys. Fluids **35**, 066601 (2023).

[7]J. A. Diez, R. Gratton, and J. Gratton, "Self-similar solution of the second kind for a convergent viscous gravity current," Phys. Fluids **4**, 1148–1155 (1992).
[8]S. Longo, M. Ungarish, V. Di Federico, L. Chiapponi, and F. Addona, "Gravity currents in a linearly stratified ambient fluid created by lock release and influx in semi-circular and rectangular channels," Phys. Fluids **28**, 096602 (2016).
[9]L. J. Marleau, M. R. Flynn, and B. R. Sutherland, "Gravity currents propagating up a slope," Phys. Fluids **26**, 046605 (2014).
[10]F. Testik and M. Ungarish, "On the self-similar propagation of gravity currents through an array of emergent vegetation-like obstacles," Phys. Fluids **28**, 056605 (2016).
[11]Z. Yan and K. N. Kowal, "A controllable sliding law for thin-film flows over slippery fluid-saturated substrates: Theory and experiments," J. Fluid Mech. **982**, A14 (2024).
[12]E. Bueler and J. Brown, "Shallow shelf approximation as a 'sliding law' in a thermomechanically coupled ice sheet model," J. Geophys. Res.: Earth Surf. **114**, F03008, https://doi.org/10.1029/2008JF001179 (2009).
[13]C. Schoof and I. Hewitt, "Ice-sheet dynamics," Annu. Rev. Fluid Mech. **45**, 217–239 (2013).
[14]C. Cottin-Bizonne, C. Barentin, É. Charlaix, L. Bocquet, and J.-L. Barrat, "Dynamics of simple liquids at heterogeneous surfaces: Molecular-dynamics simulations and hydrodynamic description," Eur. Phys. J. E **15**, 427–438 (2004).
[15]H. E. Huppert, "The propagation of two-dimensional and axisymmetric viscous gravity currents over a rigid horizontal surface," J. Fluid Mech. **121**, 43–58 (1982).
[16]H. E. Huppert, "Gravity currents: A personal perspective," J. Fluid Mech. **554**, 299–322 (2006).
[17]J. R. Lister, "Viscous flow down an inclined plane from point and line sources," J. Fluid Mech. **242**, 631–653 (1992).
[18]E. Llewellin, H. Mader, and S. Wilson, "The rheology of a bubbly liquid," Proc. R. Soc. London, Ser. A **458**, 987–1016 (2002).
[19]C. Cottin-Bizonne, S. Jurine, J. Baudry, J. Crassous, F. Restagno, and E. Charlaix, "Nanorheology: An investigation of the boundary condition at hydrophobic and hydrophilic interfaces," Eur. Phys. J. E **9**, 47–53 (2002).
[20]N. Churaev, V. Sobolev, and A. Somov, "Slippage of liquids over lyophobic solid surfaces," J. Colloid Interface Sci. **97**, 574–581 (1984).
[21]S. Mehrnia and P. F. Pelz, "Slip length of branched hydrocarbon oils confined between iron surfaces," J. Mol. Liq. **336**, 116589 (2021).
[22]J.-T. Cheng and N. Giordano, "Fluid flow through nanometer-scale channels," Phys. Rev. E **65**, 031206 (2002).
[23]J.-H. J. Cho, B. M. Law, and F. Rieutord, "Dipole-dependent slip of Newtonian liquids at smooth solid hydrophobic surfaces," Phys. Rev. Lett. **92**, 166102 (2004).